Available online at www.sciencedirect.com
ScienceDirect
Journal of Molecular Spectroscopy 244 (2007) 33–47
Journal of MOLECULAR SPECTROSCOPY
www.elsevier.com/locate/jms

High sensitivity *CW*-cavity ring down spectroscopy of N_2O near 1.5 μm (I)

A.W. Liu [a,b], S. Kassi [a], P. Malara [a,c], D. Romanini [a], V.I. Perevalov [d], S.A. Tashkun [d], S.M. Hu [b], A. Campargue [a,*]

[a] *Laboratoire de Spectrométrie Physique (associated with CNRS, UMR 5588), Université Joseph Fourier de Grenoble, B.P. 87, 38402 Saint-Martin-d'Hères Cedex, France*
[b] *Hefei National Laboratory for Physical Sciences at Microscale, University of Science and Technology of China, Hefei 230026, China*
[c] *CNR - Istituto Nazionale di Ottica Applicata (INOA), Comprensorio 'A.Olivetti', Via Campi Flegrei 34, 80078 Pozzuoli (Naples), Italy*
[d] *Laboratory of Theoretical Spectroscopy, Institute of Atmospheric Optics, SB, Russian Academy of Science, 1, Akademicheckii av., 634055, Tomsk, Russia*

Received 4 December 2006; in revised form 15 January 2007
Available online 3 February 2007

Abstract

The absorption spectrum of nitrous oxide, N_2O, in natural isotopic abundance has been recorded by CW-Cavity Ring Down Spectroscopy between 6000 and 6833 cm^{-1}. The spectra were obtained at Doppler limited resolution by using a CW-CRDS spectrometer based on a series of fibered DFB lasers. The typical sensitivity of 2×10^{-10} cm^{-1}, allowed for the detection of lines with intensity as weak as 2×10^{-29} cm/molecule while the minimum intensity value provided by HITRAN in the considered spectral region is 2×10^{-25} cm/molecule. More than 6000 line positions of five isotopologues contributing to the spectra ($^{14}N_2{}^{16}O$, $^{15}N^{14}N^{16}O$, $^{14}N^{15}N^{16}O$, $^{14}N_2{}^{18}O$ and $^{14}N_2{}^{17}O$), were measured with a typical accuracy of 1.5×10^{-3} cm^{-1} and rovibrationally assigned on the basis of their respective global effective Hamiltonian models. Highly excited rovibrational levels corresponding to J values larger than 80 could be detected for the stronger vibrational bands. The band by band analysis led to the determination of the rovibrational parameters of a total of 68 bands, 49 of them being newly reported. The rms value of the deviations of the predictions of the effective Hamiltonian models from the observed line positions is 0.010 cm^{-1}. As expected, the quality of the predictions degrades for the minor isotopologues for which important deviations up to a few wavenumbers were evidenced. Most of the bands were found unperturbed but in a few cases, local rovibrational perturbations were evidenced. The interaction mechanisms and the perturbers were univocally assigned on the basis of the effective Hamiltonian model. In particular, interpolyad couplings were evidenced indicating that the polyad version of the effective Hamiltonian has to be extended to include Coriolis and interpolyad anharmonic interactions.

Keywords: Nitrous oxide, N_2O; Near infrared; Cavity ring down spectroscopy, CRDS; Effective Hamiltonian model; 1.5 μm atmospheric window

1. Introduction

We have undertaken a systematic study of the absorption spectrum of the main atmospheric species in the 1.5 μm atmospheric transparency window by CW-Cavity Ring Down Spectroscopy (CW-CRDS): H_2O [1], $^{12}CO_2$ [2,3], $^{13}CO_2$ [3,4], and ozone [5,6]. The spectra recorded at Doppler limited resolution with a typical sensitivity of 2×10^{-10} cm^{-1}, allowed for the detection and analysis of many new transitions with intensity as weak as 5×10^{-29} cm/molecule, far beyond the sensitivity achieved by Fourier Transform spectroscopy associated with long multipass cells. The present contribution is devoted to nitrous oxide which is a greenhouse gas present in the atmosphere at a concentration around 300 ppb. Human disruptions of the nitrogen cycle are probably responsible for the steep increase of its concentration observed in recent years [7].

We will use below the HITRAN [8] notation for the different isotopologues contributing to the spectrum:

* Corresponding author. Fax: +33 4 76 63 54 95.
E-mail address: Alain.Campargue@ujf-grenoble.fr (A. Campargue).

0022-2852/$ - see front matter © 2007 Elsevier Inc. All rights reserved.
doi:10.1016/j.jms.2007.01.007

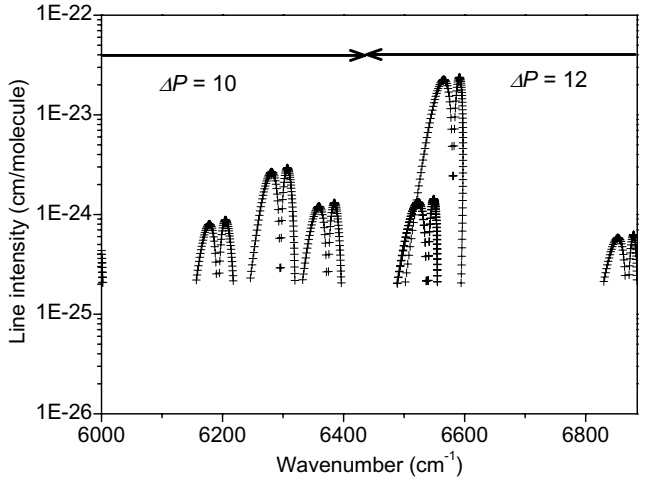

Fig. 1. Scattered spectrum of nitrous oxide as provided by the HITRAN2004 database in the 6000–6900 cm^{-1} region presently investigated by CW-CRDS. Note the logarithmic scale adopted for the line intensities. The region corresponding to the $P = 10$ and $P = 12$ polyads are roughly indicated. All the transitions are due to the $^{14}N_2{}^{16}O$ isotopologue.

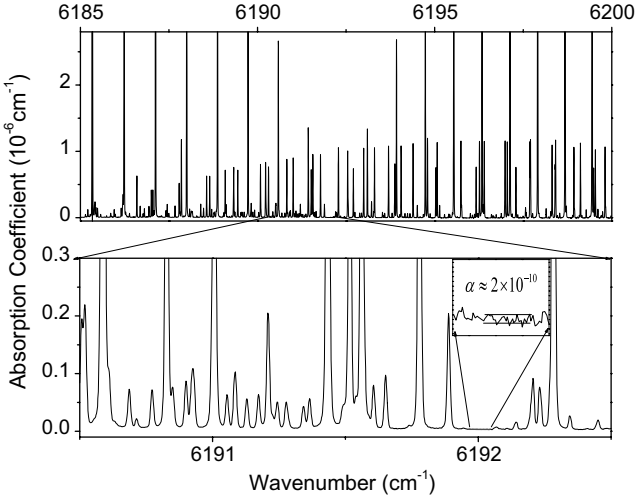

Fig. 2. CW-CRDS spectrum of natural nitrous oxide between 6185 and 6200 cm^{-1} dominated by the (10 0 10)–(0 0 1) (5000e–0000e in normal mode notation) Σ–Σ band centered at 6192.27 cm^{-1}. The sample pressure was 5.9 Torr. Two successive enlargements show the typical achieved sensitivity: the noise level corresponding to the minimum value of the absorption coefficient which can be detected is about 2×10^{-10} cm^{-1}. Note the high density of transitions observed.

$^{14}N_2{}^{16}O$: 446, $^{14}N^{15}N^{16}O$: 456, $^{15}N^{14}N^{16}O$: 546, $^{14}N_2{}^{18}O$: 448 and $^{14}N_2{}^{17}O$: 447. In the investigated spectral region, the HITRAN database [8] provides only line parameters for the 446 isotopologue, as illustrated by the overview spectrum presented in Fig. 1. The rovibrational assignments of the numerous observed transitions rely mainly on the predictions of their respective effective Hamiltonian models [9–11].

2. Experiment

2.1. The CW-CRDS spectrometer

The fibered Distributed Feed-Back (DFB) diode laser CW-CRDS spectrometer was described in details in Ref. [12]. It allows covering the 6000–6800 cm^{-1} region with the help of forty fibered DFB diode lasers, each of them having a typical tuning range of 7 nm (~30 cm^{-1}) by temperature tuning from −15 to 60 °C. The spectrum could be continuously covered except in the following narrow spectral sections: 6094.6–6131.3, 6289.1–6290.6, 6357.9–6358.3, 6528.9–6529.5, 6588.2–6597 and 6800.2–6804 cm^{-1}. A single-mode fibre delivers the laser radiation to one end of a vacuum-tight ringdown cell, which is 140 cm long. The high reflectivity ($R = 99.993\%$) cavity mirrors are mounted on tilt stages, one of which includes a piezoelectric tube. The cavity losses at each laser wavelength were obtained by averaging the results of exponential fits to a few ringdown events, thus giving one data point in the spectrum. The typical ringdown time was 60 μs. About 60 min were needed for each DFB laser in order to complete a temperature scan. The reader is referred to Refs. [4,5] for more details about the data acquisition system.

The pressure, measured by a capacitance gauge (Baratron), as well as the ringdown cell temperature (about 293 K) were continuously recorded during the experiments. Various pressures ranging between 3.5 and 12.2 Torr were adopted. In these pressure conditions, collisional broadening (FWHM ~ 2.6×10^{-3} cm^{-1} at a pressure of 10 Torr [8]) is significantly lower than Doppler broadening (FWHM ~ 11×10^{-3} cm^{-1}) and the observed line profile is mostly Gaussian as the diode laser linewidth contribution (a few MHz) is negligible.

The wavenumber calibration of the spectrum is based on the values provided by a lambdameter (Burleigh WA1640) and has been described in details in Ref. [6]. It is checked and refined by using a few reference lines for each spectral section covered by a DFB laser. We adopted the line positions of H_2O present as an impurity in the cell as reference lines. Their values were taken from HITRAN database [8]. As a result, reproducibility better than 2×10^{-4} cm^{-1} could be achieved in the overlapping part of two successive spectral regions. Maximum deviations of 2×10^{-3} cm^{-1} were observed in a few cases possibly due to the lack of accuracy of the available reference lines. This value is then claimed as maximum uncertainty on the line positions.

The achieved sensitivity is illustrated in Fig. 2. It varies from 2 to 5×10^{-10} cm^{-1} depending on the reflectivity of the mirrors. Combined with a 4–5 orders dynamics on the line intensities which can be measured, it leads to the observation of a high density of lines which made the analysis particularly laborious.

3. Rovibrational analysis

3.1. Vibrational assignment

The observed transitions were assigned on the basis of the predictions of the effective rovibrational Hamiltonian

Table 1
Observed bands and vibrational levels with the fractions respective to the bright states

Band[a]	(P, l_2, i)[b]	ΔG_v (cm^{-1})	Basis states[c]	Bright states[d]	% Fraction[e]
446 cold bands ($\Delta P = 10$)					
4200e–0000e	(10 0 9)	6058.6676	$42^0 0/010^0 0$	$50^0 0$	4.6
4220e–0000e[f] (0(10)20–0000)	(10 2 16)	6070.1332	$42^2 0/010^2 0/34^2 0$		
1800e–0000e (5000e–0000e)	(10 0 10)	6192.2711	$18^0 0/50^0 0/42^0 0$	$50^0 0$	23.4
4220e–0000e[f]	(10 2 18)	6210.2100	$42^2 0/18^2 0$		
5000e–0000e	(10 0 11)	6295.4483	$50^0 0/26^0 0$	$50^0 0/30^0 1$	52.0/1.5
3420e–0000e[f]	(10 2 20)	6333.5152	$34^2 0/26^2 0/42^2 0$		
3400e–0000e	(10 0 12)	6373.3080	$34^0 0/42^0 0/26^0 0/50^0 0$	$50^0 0$	17.1
446 cold bands ($\Delta P = 11$)					
0312e–0000e	(11 1 1)	6083.3176	$03^1 2/11^1 2$	$11^1 2$	18.1
1112e–0000e	(11 1 3)	6213.8171	$11^1 2/03^1 2$	$11^1 2$	79.7
3111e–0000e	(11 1 6)	6462.0708	$31^1 1/15^1 1/07^1 1$	$31^1 1$	43.8
3111e–0000e (2311e–0000e)	(11 1 8)	6570.7686	$31^1 1/23^1 1/15^1 1$	$31^1 1$	38.6
446 cold bands ($\Delta P = 12$)					
0003e–0000e	(12 0 1)	6580.8538	$00^0 3$	$00^0 3$	98.6
0402e–0000e	(12 0 2)	6630.4345	$04^0 2/12^0 2$	$20^0 2$	1.7
0422e–0000e[f]	(12 2 3)	6638.1707	$04^2 2/12^2 2$		
1202e–0000e	(12 0 4)	6768.5020	$12^0 2/04^0 2/20^0 2$	$20^0 2$	22.8
2002e–0000e	(12 0 6)	6868.5502	$20^0 2/12^0 2$	$20^0 2/40^0 1$	70.7/2.5
446 hot bands ($\Delta P = 10$)					
4310e–0110e	(11 1 9)	6041.8296	$43^1 0/011^1 0/27^1 0$	$51^1 0$	10.2
3201e–0200e	(12 0 12)	6046.5467	$32^0 1/40^0 1/24^0 1$		
5200e–1000e	(12 0 13)	6055.8898	$52^0 0/012^0 0/36^0 0$		
5310e–0310e	(13 1 13)	6164.0633	$53^1 0/013^1 0/61^1 0$		
5200e–0200e	(12 0 13)	6172.6617	$52^0 0/012^0 0/36^0 0$		
5220e–0220e	(12 2 23)	6177.2886	$52^2 0/36^2 0/012^2 0/110^2 0$		
6000e–1000e (4400e–1000e)	(12 0 14)	6179.0824	$60^0 0/44^0 0/110^0 0$		
5110e–0110e (1910e–0110e)	(11 1 10)	6183.7524	$51^1 0/19^1 0/35^1 0/011^1 0$	$51^1 0$	32.8
6000e–1000e	(12 0 15)	6271.2321	$60^0 0/52^0 0$		
6000e–0200e (4400e–0200e)	(12 0 14)	6295.8535	$60^0 0/44^0 0/110^0 0$		
5110e–0110e	(11 1 11)	6303.4589	$51^1 0/19^1 0/27^1 0$	$51^1 0/31^1 1$	41.7/1.3
5220e–0220e (1(10)20e–0220e)	(12 2 25)	6310.8843	$52^2 0/110^2 0/44^2 0$		
4400e–1000e (3600e–1000e)	(12 0 16)	6355.5726	$44^0 0/36^0 0/52^0 0/28^0 0$		
3710e–1110e	(13 1 16)	6386.0202	$37^1 0/45^1 0/29^1 0$		
6000e–0200e	(12 0 15)	6388.0022	$60^0 0/52^0 0$		
3510e–0110e	(11 1 12)	6407.2488	$35^1 0/43^1 0/27^1 0$	$51^1 0$	11.6
3620e–0220e	(12 2 27)	6432.8729	$36^2 0/44^2 0/28^2 0$		
4400e–1000e (3600e–0200e)	(12 0 16)	6472.3431	$44^0 0/36^0 0/52^0 0/28^0 0$		
446 hot bands ($\Delta P = 11$)					
1222e–0110e	(12 2 7)	6191.587	$12^2 2/04^2 2$		
446 hot bands ($\Delta P = 12$)					
0443e–0440e	(16 4 4)	6412.2145	$04^4 3$		
0423e–0420e	(16 2 3)	6415.4688	$04^2 3/12^2 3$		
0403e–0400e	(16 0 2)	6416.7323	$04^0 3/12^0 3$		
0333e–0330e	(15 3 2)	6453.8973	$03^3 3$		
1113e–1110e	(15 1 3)	6455.5313	$11^1 3/03^1 3$		
0313e–0310e	(15 1 1)	6456.2032	$03^1 3/11^1 3$		
0004e–0001e	(16 0 1)	6490.3825	$00^0 4$		
0223e–0220e	(14 2 2)	6495.8908	$02^2 3$		
0203e–0200e	(14 0 1)	6497.1408	$02^0 3$		
1003e–1000e	(14 0 3)	6497.7584	$10^0 3$		
0113e–0110e	(13 1 1)	6538.2111	$01^1 3$	$01^1 3$	98.6
0622e–0220e	(14 2 4)	6551.9537	$06^2 2/14^2 2$		
0602e–0200e	(14 0 2)	6554.4597	$06^0 2/14^0 2$		
0512e–0110e	(13 1 2)	6590.5682	$05^1 2/13^1 2$	$21^1 2$	4.0
2112e–0110e (0512e–0110e)	(13 1 4)	6736.8466	$21^1 2/05^1 2/13^1 2$	$21^1 2/41^1 1$	33.5/1.3
456 cold bands ($\Delta P = 10$)					
4200e –0000e	(10 0 10)	6121.7313	$42^0 0/26^0 0/18^0 0$	$50^0 0/30^0 1$	6.3/1.9
5000e–0000e (3400e–0000e)	(10 0 11)	6240.6649	$50^0 0/34^0 0/26^0 0$	$50^0 0/30^0 1$	32.5/8.1
5000e–0000e	(10 0 12)	6322.9984	$50^0 0/42^0 0$	$50^0 0/30^0 1$	41.0/8.9

(*continued on next page*)

Table 1 (*continued*)

Band[a]	(P, l_2, i)[b]	ΔG_v (cm^{-1})	Basis states[c]	Bright states[d]	% Fraction[e]
456 cold bands ($\Delta P = 12$)					
0003e–0000e	(12 0 1)	6446.8942	00^03	$00^03/20^02$	93.5/6.1
1202e–0000e	(12 0 5)	6653.9461	12^02	$20^02/40^01$	6.6/2.0
2002e–0000e	(12 0 7)	6775.2218	$20^02/40^01$	$20^02/40^01/00^03/60^00$	63.4/19.4/5.3/1.9
456 hot band ($\Delta P = 12$)					
0113e–0110e	(13 1 2)	6406.4232	01^13	$01^13/21^12$	93.9/5.6
546 cold bands ($\Delta P = 10$)					
0(10)00e–0000e	(10 0 10)	6135.3659	$010^00/50^00/34^00$	50^00	27.7
5000e–0000e	(10 0 11)	6232.9173	$50^00/18^00$	50^00	48.3
3400e–0000e	(10 0 12)	6315.0165	$34^00/26^00/42^00$	50^00	13.7
546 cold bands ($\Delta P = 12$)					
0003e–0000e	(12 0 1)	6515.9876	00^03	00^03	100
0402e–0000e	(12 0 5)	6702.3528	$04^02/12^00/20^02$	20^02	30.4
2002e–0000e	(12 0 6)	6795.9326	$20^02/12^02$	20^02	66.7
546 hot band ($\Delta P = 12$)					
0113e–0110e	(13 1 1)	6473.4353	01^13	01^13	100
448 cold bands ($\Delta P = 10$)					
5000e–0000e	(10 0 11)	6140.5548	$50^00/26^00$	50^00	58.2
448 cold bands ($\Delta P = 12$)					
0003e–0000e	(12 0 1)	6558.6737	00^03	00^03	100
1202e–0000e	(12 0 4)	6702.9328	$12^02/20^02/04^02$	20^02	25.2
447 cold bands ($\Delta P = 12$)					
0003e–0000e	(12 0 1)	6569.4882	00^03	00^03	100

[a] $V_1 V_2^{l_2} V_3$. According to the maximum value of the modulo of the expansion coefficients of the eigenfunction. In the cases when there are two candidates for the same labeling or when the modulo of two principal expansion coefficients practically coincide, we give in parentheses the second variant of the labeling.

[b] Cluster labelling notation: $(P = 2V_1 + V_2 + 4V_3, \ell_2, i)$ for the upper state of the band; i is the order number within the cluster increasing with the energy.

[c] Only basis states with modulo of expansion coefficients larger than 0.4 are presented. We use different notations for an eigenstate $V_1 V_2^{l_2} V_3$ and for a basis state $V_1 V_2 l_2 V_3$.

[d] Bright states are given only for the bands originating from ground vibrational state and from the first excited vibrational state 0110.

[e] Square of the expansion coefficient of the vibrational state relative to the bright basis states appearing in the eigenfunction expansion with a fraction larger than 0.01.

[f] Fractions of the bright states are strongly J dependent.

developed by Teffo et al. [9–11]. This model is based on a polyad structure resulting from the approximate relations between the harmonic frequencies $\omega_3 \approx 2\omega_1 \approx 4\omega_2$. As the mixing between the $V_1 V_2^{l_2} V_3$ states may be strong, the energy levels are preferably labeled using the triplet $\{P = 2V_1 + V_2 + 4V_3, l_2, i\}$ where the index i increases with the energy. As a general rule, the transition moment of a given transition is much weaker when the bending quantum numbers of the lower and upper states differ. In consequence, cold bands are dominated by transitions reaching upper vibrational states with important fractions of pure stretching states $V_1 0^0 V_3$ which are then considered as bright states. The same is true for the $V_1 1^0 V_3$ upper states which can be considered as the bright states of the hot bands originating from the $(0\ 1^1 0)$ bending state. The vibrational assignment and fraction relative to these bright states are given in Table 1 for the presently studied levels.

As illustrated in Fig. 1, the absorption in the studied region is dominated by cold bands reaching the $P = 10$ and $P = 12$ polyads which are observed below and above $6500\ \mathrm{cm}^{-1}$, respectively. More precisely, the upper states of the cold bands observed between 6000 and $6500\ \mathrm{cm}^{-1}$ belong to a subset of states of the $P = 10$ polyad associated with the (50^00) bright state while the $P = 12$ upper states observed between 6500 and $6900\ \mathrm{cm}^{-1}$ correspond to important fractions of the (00^03) and (20^02) bright states. Many hot bands with $\Delta P = 10$ and $\Delta P = 12$ associated to the above cold bands could be detected. For instance, hot bands corresponding to an excitation of states of the $P = 16$ polyad from states of the $P = 4$ polyad around $2300\ \mathrm{cm}^{-1}$, could be detected while their relative population is on the order of 10^{-5} leading to line intensities on the order of 10^{-29}–10^{-28} cm/molecule. It is worth mentioning that except four $\Delta P = 10$ Σ–Δ cold bands, four $\Delta P = 11$ Σ–Π cold bands and one $\Delta P = 11$ Π–Δ hot band, all the other

analysed bands are parallel bands ($\Delta l_2 = 0$): 22 Σ–Σ bands, 11 Π–Π bands, 6 Δ–Δ bands, one Φ–Φ band and one Γ–Γ band.

The overall situation is similar for the 456 and 546 isotopologues, for which six Σ–Σ cold bands are reported for both species. As a consequence of the 3.64×10^{-3} relative abundance of these isotopologues, only the Π–Π hot band associated to the strong $3\nu_3$ band could be detected.

Finally, three Σ–Σ bands of the 448 isotopologue (1.98×10^{-3} relative abundance) and the $3\nu_3$ Σ–Σ band of the 447 isotopologue (3.69×10^{-4} relative abundance) were identified.

The comparison of the observed spectrum with both HITRAN2004 and the predictions of the effective rovibrational Hamiltonian are illustrated in Figs. 3 and 4. The density of detected lines is typically 10–20 lines/cm^{-1}, which makes difficult the assignment process.

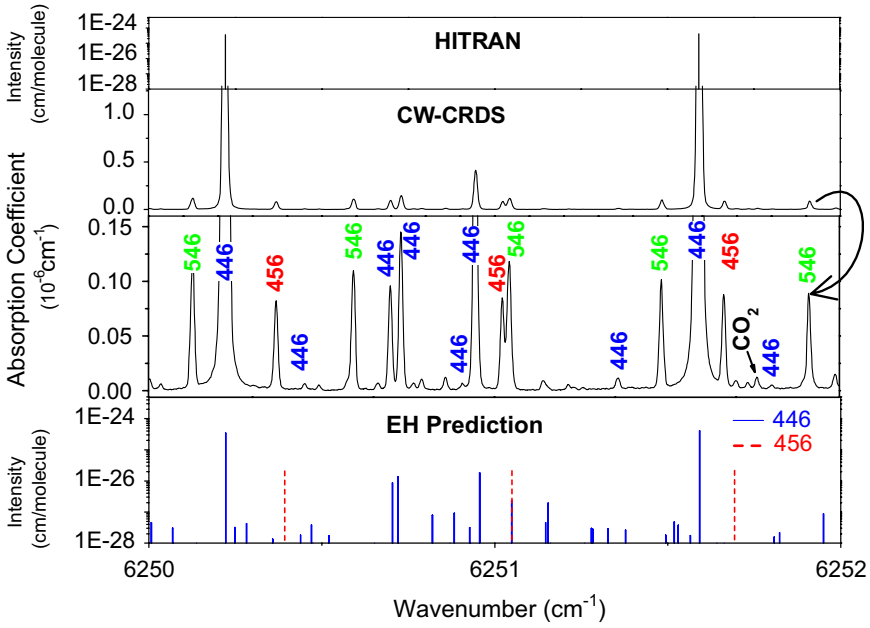

Fig. 3. Comparison of the absorption spectrum of nitrous oxide in a 2 cm^{-1} spectral section around 6251 cm^{-1}. Three isotopologues in natural abundance contribute to the observed spectrum. (a) Stick spectrum of carbon dioxide in natural abundance as provided by HITRAN2004 [8], (b) CW-CRDS spectrum recorded with a pressure of 12.0 Torr, (c) same as (b) with an enlargement factor of about 10 for the absorbance scale, (d) stick spectrum of the 446 and 456 isotopologues contributing to the observed transitions as predicted by the effective Hamiltonian models [9–11]. Note the logarithmic scale adopted in (a) and (d) for the line intensities.

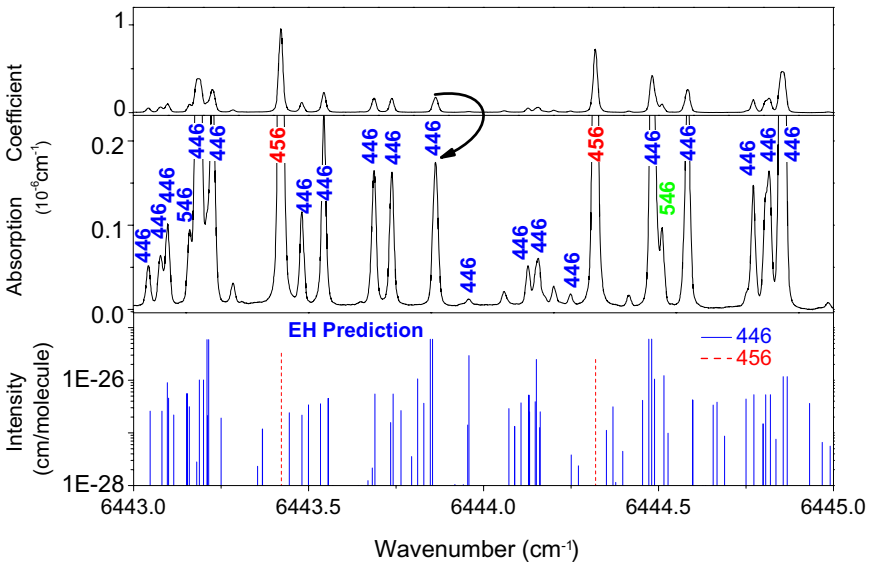

Fig. 4. Same as Fig. 3 in the 6443–6445 cm^{-1} spectral region. No transitions are provided by the HITRAN database in the considered spectral region.

Table 2
Spectroscopic parameters (in cm^{-1}) of the rovibrational bands of $^{14}N_2{}^{16}O$ recorded by *CW*-CRDS between 6000 and 6833 cm^{-1}

Lower states constants [15]

State		G_v	B_v	$D_v \times 10^7$	$H_v \times 10^{12}$
$V_1 V_2^{l_2} V_3$	(P, l_2, i)				
0000e	(0 0 1)	0.0	0.419 011 001	1.760919	−0.016529
0110*e*	(1 1 1)	588.76787	0.419 177 925	1.783245	−0.01714
0110f		588.76787	0.419 969 845	1.793030	−0.01766
0200e	(2 0 1)	1168.1323	0.419 920 952	2.491945	2.955393
0220e	(2 2 2)	1177.74467	0.420 125 256	1.196792	−2.950211
0220f		1177.74467	0.420 126 260	1.818000	0.095
1000e	(2 0 2)	1284.90334	0.417 255 210	1.726978	0.146666
0310f		1749.06515	0.421 079 073	2.177366	−0.35921
0310e	(3 1 1)	1749.06523	0.419 583 944	2.110353	1.2225
0330e	(3 3 2)	1766.91238	0.420 667 053	1.617863	−0.99132
1110e	(3 1 2)	1880.26574	0.417 464 677	1.748503	0.10750
1110f		1880.26574	0.418 372 995	1.719561	0.21746
0001e	(4 0 1)	2223.75677	0.415 559 510	1.754675	−0.013626
0400e	(4 0 2)	2322.57308	0.420 618 918	3.964712	14.029
0420f		2331.12145	0.420 772 247	2.16104	0.48397
0420e	(4 2 3)	2331.12151	0.420 768 064	0.173512	−14.293
0440e	(4 4 4)	2356.25242	0.421 218 620	2.7201	171.28

ΔG_v[a]	Type	$V_1 V_2^{l_2} V_3$ [b]	(P, l_2, i)	G_v	B_v	$D_v \times 10^7$	$H_v \times 10^{12}$	Observed lines	n/N[c]	rms $\times 10^3$	Previous reports[d]
Cold Bands											
6058.66761(15)	Σ–Σ	4200e–0000e	(10 0 9)	6058.66761(15)	0.41731504(65)	5.7144(62)	31.02(16)	P54/R50	103/105	0.7	
		4200e–0000e[Wa]		*6058.67008(80)*	*0.4172870(34)*	*5.129(27)*		*P37/R36*	*71/86*	*3.4*	
		2600e– 0000e[T]		*6058.66749(8)*	*0.4173112 (61)*	*5.652(89)*	*29.8(43)*				
6070.13318(91)	Δ–Σ	4220e–0000e	(10 2 16)	6070.13318(91)	0.4176012(24)	−0.946(17)	−29.28(34)	P57/R29	48/49	1.1	
		(0(10)20e–0000e)									
6083.31762(21)	Π–Σ	0312e-0000e	(11 1 1)	6083.31762(21)	0.4129306(7)	2.0627(37)	[−0.016529]	P47/R14	48/48	0.9	*0312–0110*[Wa]
6083.31688(26)		0312f-0000e		6083.31688(26)	0.4143755(6)	2.1886(27)	[−0.016529]	Q50	43/43	0.9	
6192.27105(13)	Σ–Σ	1800e–0000e	(10 0 10)	6192.27105(13)	0.414927182(37)	3.4326(24)	7.877(41)	P55/R64	115/118	0.6	
		3400e–0000e[T]		*6192.27059(26)*	*0.41493015(32)*	*3.4674(29)*	*8.908(20)*				
6210.21003(57)	Δ–Σ	4220e–0000e	(10 2 18)	6210.21003(57)	0.4156528(10)	0.7112(53)	−8.298(77)	P56/R65	62/76	0.8	*3420e-0220e*[T]
6213.81711(19)	Π–Σ	1112e–0000e	(11 1 3)	6213.81711(19)	0.4106262(3)	1.7176(11)	[−0.016529]	P61/R54	100/104	1.0	*1112e-0110e*[T]
6213.81738(32)		1112f–0000e		6213.81738(32)	0.4114883(6)	1.6908(23)	[−0.016529]	Q55	52/53	1.2	*1112f-0110f*[T]
		1112–0000[Wa]						P28/Q34/R33	47/58	3.1	
6295.44831(16)	Σ–Σ	5000e–0000e	(10 0 11)	6295.44831(16)	0.41241166(38)	2.1838(19)	4.620(26)	P65/R71	104/108	0.7	
		4200e–0000e[T]		*6295.44763(10)*	*0.41240934(36)*	*2.15906(39)*	*4.087(27)*				
6333.51524(89)	Δ–Σ	3420e–0000e	(10 2 20)	6333.51524(89)	0.4144959(18)	1.3910(97)	−5.77(16)	P63/R53	56/60	1.0	*4220e-0220e*[T]
6373.30804(20)	Σ–Σ	3400e–0000e	(10 0 12)	6373.30804(20)	0.41234755(50)	0.5586(27)	6.280(39)	P66/R70	121/127	1.0	
		5000e–0000e[T]		*6373.30771(23)*	*0.41234525(46)*	*0.5262(59)*	*5.16(18)*				
6462.07080(93)	Π–Σ	3111e–0000e	(11 1 6)	6462.07080(93)	0.4126063(39)	2.01(35)	[−0.016529]	P32/R25	18/18	1.0	*2311e-0110e*[T]
6462.0717(18)		3111f–0000e		6462.0717(18)	0.4143027(40)	2.067(17)	[−0.016529]	Q33	8/8	2.0	*2311 f -0110f*[T]
6570.76861(61)	Π–Σ	3111e–0000e	(11 1 8)	6570.76861(61)	0.4109654(15)	1.4801(70)	[−0.016529]	P47/R12	19/20	1.1	*3111e-0110e*[T]
		(2311e–0000e)									
6570.7664(18)		3111f–0000e		6570.7664(18)	0.4122536(51)	1.587(30)	[−0.016529]	Q40	14/14	2.1	*3111 f -0110f*[T]
		(2311f–0000e)									

6580.85384(18)	Σ–Σ	0003e–0000e	(12 0 1)	6580.85384(18)	0.40863530(20)	1.74548(31)	[−0.016529]	P81/R82	118/123	1.2	
		0003e–0000e^{T}		*6580.85370(5)*	*0.408635527(6)*	*1.74541(15)*					
		0003e–0000e^{We}		*6580.85422(29)*	*0.40863483(63)*	*1.7418(31)*	*−0.109(39)*		*108/114*	*1.5*	
6630.43452(15)	Σ–Σ	0402e–0000e	(12 0 2)	6630.43452(15)	0.41401486(55)	3.9837(45)	15.767(98)	P53/R57	91/93	0.7	
		0402e–0000e^{We}		*6630.43543(5)*	*0.4139944(17)*	*3.619(11)*	*[−0.01555]*			*2.2*	
6638.1707(14)	Δ–Σ	0422e–0000e	(12 2 3)	6638.1707(14)	0.4142175(30)	0.645(14)	[−0.016529]	P39/R45	36/42	2.0	
6768.50202(14)	Σ–Σ	1202e–0000e	(12 0 4)	6768.50202(14)	0.41136786(41)	2.4127(27)	2.785(44)	P66/R64	118/129	0.7	
		1202e– 0000e^{T}		*6768.50167(96)*	*0.4113657(13)*	*2.391(12)*	*5.05(23)*				
		1202e– 0000e^{We}		*6768.50258(33)*	*0.4113665(13)*	*2.406(18)*	*26.7(53)*			*1.4*	
6868.550165(89)	Σ–Σ	2002e–0000e	(12 0 6)	6868.550165(89)	0.4086249(1)	1.60282(38)	0.608(62)	P67/R35	99/99	0.5	
		2002e– 0000e^{T}		*6868.54982(50)*	*0.40862919(96)*	*1.698(19)*	*5.89(85)*				
		2002e– 0000e^{We}		*6868.55062(28)*	*0.4086257(14)*	*1.631(16)*	*1.76(48)*		*96/97*	*1.2*	
Hot bands											
6041.82958(23)	Π–Π	4310e–0110e	(11 1 9)	6630.59745(23)	0.41593896(98)	3.1369(98)	7.09(26)	P41/R51	83/85	0.9	
6041.82729(33)		4310f–0110f		6630.59516(33)	0.41913870(64)	3.5234(22)	[−0.01766]	P45/R56	91/92	1.7	
		4310–0110^{Wa}						*P27/R27*	*56/73*	*3.2*	
6046.54666(31)	Σ–Σ	3201e–0200e	(12 0 12)	7214.67896(31)	0.4096191(12)	0.9624(81)	[2.955393]	P37/R39	68/70	1.3	*4001e– 0000e*^{T}
											4001e– 0000e^{We}
6055.88976(49)	Σ–Σ	5200e–1000e	(12 0 13)	7340.79310(49)	0.4152574(26)	4.919(22)	[0.146666]	P37/R33	53/53	1.9	*5200e– 0000e*^{Wa}
6164..06334(55)	Π–Π	5310e–0310e	(13 1 13)	7913.12857(55)	0.4138092(44)	3.109(62)	[1.2225]	P23/R26	23/25	1.4	
6164.06256(62)		5310f–0310f		7913.12771(62)	0.4171901(47)	3.436(61)	[−0.35921]	P29/R25	29/29	1.7	
6172.66175(44)	Σ–Σ	5200e–0200e	(12 0 13)	7340.79405(44)	0.4152543(17)	4.905(12)	[2.955393]	P39/R38	70/70	1.9	
6177.28856(37)	Δ–Δ	5220e–0220e	(12 2 23)	7355.03323(37)	0.4157309(15)	−0.633(14)	−24.52(33)	P42/R53	71/75	1.3	
6177.29119(33)		5220f–0220f		7355.03586(33)	0.4157274(10)	2.4237(58)	[0.095]	P43/R42	66/74	1.3	
6179.08236(25)	Σ–Σ	6000e–1000e (4400e–1000e)	(12 0 14)	7463.98570(25)	0.4128004(12)	3.284(13)	7.64(38)	P44/R49	77/83	1.0	*6000e– 0000e*^{We}
6183.75236(21)	Π–Π	5110e–0110e (1910e–0110e)	(11 1 10)	6772.52023(21)	0.4139682(62)	2.4022(33)	[−0.01714]	P47/R43	82/90	1.0	
6183.75212(24)		5110f–0110f (1910f–0110f)		6772.51999(24)	0.4166002(43)	2.5907(14)	[−0.01766]	P49/R60	93/103	1.3	
		5110–0110^{Wa}						*P41/R29*	*63/92*	*3.0*	
6191.58731(37)	Δ–Π	1222e–0110e	(12 2 7)	6780.35518(37)	0.4117679(10)	1.2754(57)	[−0.01714]	P46/R39	53/56	1.2	
6191.58704(53)		1222e–0110f		6780.35491(53)	0.4117693(12)	1.2833(54)	[−0.01766]	Q49	35/36	1.5	
6191.58863(51)		1222f–0110e		6780.35650(51)	0.4117616(12)	1.7191(52)	[−0.01714]	Q49	30/30	1.3	
6191.58800(42)		1222f–0110f		6780.35587(42)	0.4117633(11)	1.7304(56)	[−0.01766]	P47/R35	51/52	1.3	
6271.23212(23)	Σ–Σ	6000e–1000e	(12 0 15)	7556.13546(23)	0.4106592(12)	1.623(13)	7.79(38)	P41/R48	75/82	0.9	*6000e– 0000e*^{O}
6295.85347(25)	Σ–Σ	6000e–0200e (4400e–0200e)	(12 0 14)	7463.98577(25)	0.4127959(93)	3.1836(63)	[2.955393]	P41/R39	65/66	1.1	*6000e– 0000e*^{We}
6303.45899(53)	Π–Π	5110e–0110e (perturbed)	(11 1 11)	6892.22686(53)	0.4122810(11)	1.6830(49)	[−0.01714]	P49/R50	72/116	2.0	
6303.45742(56)		5110f–0110f		6892.22529(56)	0.4143919(76)	1.6665(23)	[−0.01766]	P48/R62	63/107	1.9	
		5110–0110^{Wa}						P30/R46	45/95	2.9	
6310.88428(29)	Δ–Δ	5220e–0220e (1(10)20e–0220e)	(12 2 25)	7488.62895(29)	0.4140482 (14)	0.833(15)	−11.00(43)	P47/R48	71/80	1.0	
6310.88512(48)		5220f–0220f (1(10)20f–0220f)		7488.62979(48)	0.4140547(13)	1.7795(68)	[0.095]	P47/R45	74/76	2.0	
6355.57263(36)	Σ–Σ	4400e–1000e (3600e–1000e)	(12 0 16)	7640.47597(36)	0.4118361(12)	−0.3028(74)	[0.146666]	P34/R50	72/77	1.7	
6386.02024(99)	Π–Π	3710e–1110e	(13 1 16)	8266.28598(99)	0.4107744(72)	0.33(10)	[0.10750]	P26/R26	25/25	2.3	
6386.01762(49)		3710f–1110f		8266.28336(49)	0.4133900(38)	0.368(57)	[0.21746]	P27/R24	31/32	1.2	
6388.00221(51)	Σ–Σ	6000e–0200e	(12 0 15)	7556.13451(51)	0.4106637(36)	1.638(49)	[2.955393]	P27/R26	28/29	1.3	*6000e– 0000e*^{We}
											6000e– 0000e^{O}

(*continued on next page*)

Table 2 (*continued*)

ΔG_v[a]	Type	$V_1 V_2^{l_2} V_3$ [b]	(P, l_2, i)	G_v	B_v	$D_v \times 10^7$	$H_v \times 10^{12}$	Observed lines	n/N[c]	rms $\times 10^3$	Previous reports[d]
6407.24884(14)	Π–Π	3510e–0110e	(11 1 12)	6996.01671(14)	0.41188264(50)	1.2127(40)	3.055(83)	P54/R57	99/123	0.6	
6407.24876(16)		3510f–0110f		6996.01663(16)	0.41394201(56)	0.7149(45)	2.306(97)	P59/R53	102/125	0.7	
		3510–0110^{Wa}						*P25/R41*	*66/103*	*3.0*	
6412.21453(70)	Γ–Γ	0443e–0440e	(16 4 4)	8768.46695(70)	0.4113087(15)	[2.7201]	[171.28]	P13/R30	20/21	1.9	
6415.46877(66)	Δ–Δ	0423e–0420e	(16 2 3)	8746.59028(66)	0.4108732(16)	0.173512	[−14.293]	P16/R28	24/25	2.0	
6415.46970(53)		0423f–0420f		8746.59121(53)	0.4108768(21)	2.16104	[0.48397]	P16/R28	22/23	1.5	
6416.73231(33)	Σ–Σ	0403e–0400e	(16 0 2)	8739.30539(33)	0.41069080(64)	3.964712	[14.029]	P16/R33	23/24	1.1	
6432.87289(42)	Δ–Δ	3620e–0220e	(12 2 27)	7610.61756(42)	0.4134222(12)	1.8844(57)	[−2.950211]	P49/R46	72/74	2.1	
6432.87279(32)		3620f–0220f		7610.61746(32)	0.41340460(84)	0.9951(38)	[0.095]	P49/R49	73/75	1.6	
6453.89733(62)	Φ–Φ	0333e–0330e (perturbed)	(15 3 2)	8220.80971(62)	0.4106339(15)	1.5564(79)	[−0.99132]	P42/R46	56/83	2.2	
6455.52903(42)	Π–Π	1113f–1110f	(15 1 3)	8335.79477(42)	0.40804620(56)	1.719561	[0.21746]	P42/R36	48/63	1.9	*1113– 0110*^{O}
6455.53130(43)		1113e–1110e		8335.79704(43)	0.40720270(58)	1.748503	[0.10750]	P42/R38	53/64	2.1	
6456.20296(32)	Π–Π	0313f–0310f	(15 1 1)	8205.26811(32)	0.41102130(45)	[2.177366]	[−0.35921]	P42/R37	69/72	1.8	*0313–0110*^{O}
6456.20321(30)		0313e–0310e		8205.26844(30)	0.40960540(40)	[2.110353]	[1.2225]	P43/R39	64/70	1.6	
6472.34307(46)	Σ–Σ	4400e–0200e (3600e–0200e)	(12 0 16)	7640.47537(46)	0.4118356(13)	−0.2703(68)	[2.955393]	P36/R46	46/47	1.7	*4400e– 0000e*^{O}
6490.38253(43)	Σ–Σ	0004e–0001e	(16 0 1)	8714.13930(43)	0.4051885(12)	1.7910(64)	[−0.013626]	P43/R45	51/52	1.6	*0004e– 0000e*^{We}
6495.89195(37)	Π–Π	0223f–0220f		7673.63662(37)	0.40998160(61)	1.8018(17)	[0.095]	P63/R60	98/124	2.0	
6495.89077(31)		0223e–0220e	(14 2 2)	7673.63544(31)	0.40998630(50)	1.1877(14)	[−2.950211]	P64/R60	100/123	1.7	
		0223–0220^{We}							*62/67*	*3.3*	
6497.14085(19)	Σ–Σ	0203e–0200e	(14 0 1)	7665.27315(19)	0.4097826(46)	2.4897(21)	[2.955393]	P41/R50	81/84	1.0	*0203e– 0000e*^{O}
		0203e– 0200e^{We}		*7665.27623(40)*	*0.4097778(14)*	*2.4282(90)*	*[−0.1555]*			*1.9*	
6497.75836(25)	Σ–Σ	1003e–1000e	(14 0 3)	7782.66170(25)	0.40682510(60)	1.7070(25)	[0.146666]	P52/R48	76/82	1.2	*1003e– 0000e*^{T}
											1003e– 0000e^{O}
											1003e– 0000e^{We}
6538.211101(86)	Π–Π	0113e–0110e	(13 1 1)	7126.978971(86)	0.40893630(11)	1.76359(24)	[−0.01714]	P70/R75	110/111	0.5	*0113e– 0110e*^{T}
		0113e– 0110e^{T}		*7126.97880(14)*	*0.40968993(16)*	*1.78673(91)*					
6538.21118(14)		0113f–0110f		7126.97905(14)	0.40968890(17)	1.78142(35)	[−0.01766]	P72/R75	116/117	0.9	*0113f– 0110 f*^{T}
		0113f– 0110 f^{T}		*7126.97881(24)*	*0.40893689(21)*	*1.7644(15)*					
		0113–0110^{We}							*154/174*	*2.7*	
6551.9537(12)	Δ–Δ	0622e–0220e	(14 2 4)	7729.69837(12)	0.4148811(88)	−1.17(13)	[−2.950211]	P19/R24	19/20	1.9	
6551.9565(14)		0622f–0220f		7729.70117(14)	0.414891(12)	2.96(20)	[0.095]	P21/R23	17/17	2.1	
6554.4597(14)	Σ–Σ	0602e–0200e	(14 0 2)	7722.5920(14)	0.4147066(66)	5.495(56)	[2.955393]	P35/R30	20/21	2.8	
6590.56819(51)	Π–Π	0512e–0110e	(13 1 2)	7179.33606(51)	0.413367(12)	2.4305(54)	[−0.01714]	P39/R48	56/60	1.7	
6590.56474(65)		0512f–0110f		7179.33261(65)	0.4154712(09)	2.8088(40)	[−0.01766]	P35/R48	65/65	1.4	
6736.84656(28)	Π–Π	1312e–0110e	(13 1 4)	7325.61443(28)	0.41109860(56)	2.0263(21)	[−0.01714]	P56/R54	95/103	1.4	
6736.84489(28)		1312f–0110f		7325.61276(28)	0.41263770(55)	2.1361(20)	[−0.01766]	P55/R55	98/102	1.4	
		1312–0110^{We}							*72/104*	*3.6*	

Notes. The cold and hot bands are listed successively and ordered according to their ΔG_v values. When a given band has been previously analyzed, the corresponding spectroscopic parameters are given in italics for comparison: ^{T}Toth [15], ^{We}Weirauch et al. [16], ^{O}Oshika et al. [17], and ^{Wa}Wang et al. [18]. The lower state constants and those appearing between square brackets were held fixed at the values of Ref. [15]. The uncertainties are given in parenthesis in the unit of the last quoted digit.

[a] Difference between the upper and lower vibrational term values.

[b] Normal mode labeling according to the maximum value of the modulo of the expansion coefficients of an eigenfunction. In the cases when there are two candidates for the same labeling or when the modulo of two principal expansion coefficients practically coincide, we give in parentheses the second variant of the labeling. Note that, as a result of strong vibrational mixing, the normal mode labeling of some states differs from that given in the previous analysis.

[c] n, number of transitions included in the fit; N, number of assigned rotational transitions.

[d] Previous observations of the upper level through a different transition.

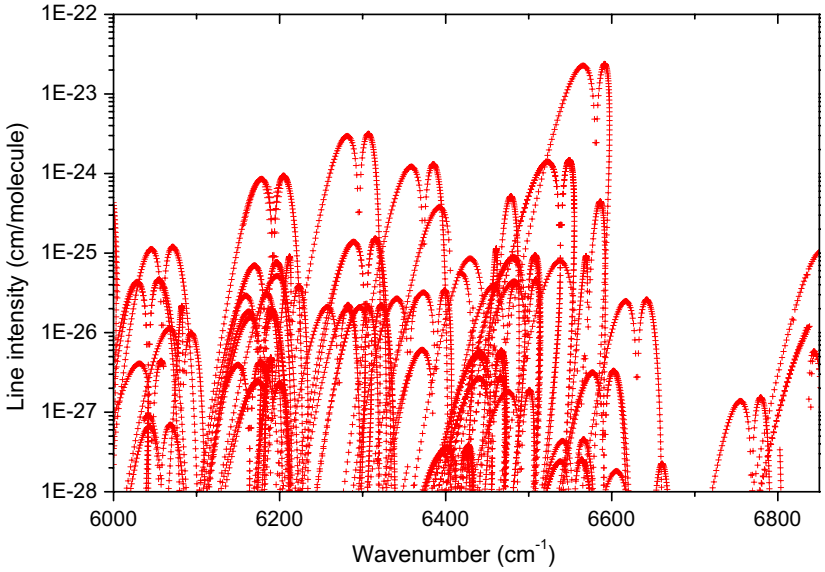

Fig. 5. Overview of the transitions assigned for the main isotopologue, $^{14}N_2{}^{16}O$, of nitrous oxide between 6000 and 6833 cm^{-1}. For the line intensities, we have adopted the values predicted by the effective Hamiltonian models [10] with the effective dipolar momentum of Ref. [21]. A logarithmic scale is used for the line intensities.

3.2. Band by band rotational analysis

In the case of unperturbed bands, the rotational analysis was performed using the standard equation for the vibration-rotation energy levels:

$$F_v(J) = G_v + B_vJ(J+1) - D_vJ^2(J+1)^2 + H_vJ^3(J+1)^3, \quad (1)$$

where G_v is the vibrational term value, B_v is the rotational constant, D_v and H_v are centrifugal distortion constants. The spectroscopic parameters were fitted directly to the observed wavenumbers and, in the case of hot bands involving *e* and *f* rotational levels, the *ee*, *ef*, *fe* and *ff* sub bands were considered independently. The lower state rotational constants were constrained to their literature values. The observed and calculated line positions are included in the Supplementary Material attached to this paper.

3.2.1. The $^{14}N_2{}^{16}O$ isotopologue

Fifty bands of the $^{14}N_2{}^{16}O$ isotopologue could be identified. The spectroscopic parameters retrieved from the fit of the line positions are listed in Table 2. The rms value of the (obs.-calc.) deviations are generally on the order of 1.5×10^{-3} cm^{-1} which is consistent with the uncertainty on the line positions. In a few cases corresponding to the strongest transitions, saturation effect prevents an accurate determination of the CRDS line positions. In this situation, in order to have a complete input data set for the parameters determination, we adopted previously published FTS line positions (as marked in the Supplementary Material).

We present in Fig. 5 an overview of all the transitions which were assigned to the 446 isotopologue. The comparison with the HITRAN database (Fig. 1) [8] together with the literature review show that the present results represent a considerable extension to the knowledge of the absorption spectrum near 1.5 μm. 5116 lines were assigned for the 446 main isotopologue while, in the studied spectral region, the HITRAN2004 database being based on the SISAM.N2O line list established by Toth [13], provides less than 600 lines (see Fig. 1) for nitrous oxide. Indeed, only a few of the observed bands have been previously detected by Fourier transform spectroscopy (FTS) associated with long multipass cells. In their pioneer work, Amiot and Guelachvili reported the four stronger Σ–Σ bands of the region [14]. More recently, Toth retrieved accurate rovibrational parameters of four additional bands detected with an absorption path length up to 422 meters [15]. These observations were completed by Weirauch et al. [16] who reported four new bands. Finally and very recently, Wang et al. [18] could newly detect four Π–Π bands and one Π–Σ band from their FTS spectrum recorded with a 105 m path length. Then, a total of seventeen bands (marked in Table 2) were previously known. The CW-CRDS sensitivity allows both for detecting 33 additional bands and increasing to higher *J* values the transitions observed in the rotational structure of the previously reported bands. We have reviewed and included in Table 2, the spectroscopic parameters of the upper vibrational states when reported from previous analysis of the same bands. It is worth mentioning that a few of the upper levels presently detected, have been previously observed in different spectral regions through transitions from different lower states. This is in particular the case of some levels detected by frequency modulation diode spectroscopy around 1.3 μm [17]. For completeness, we have also

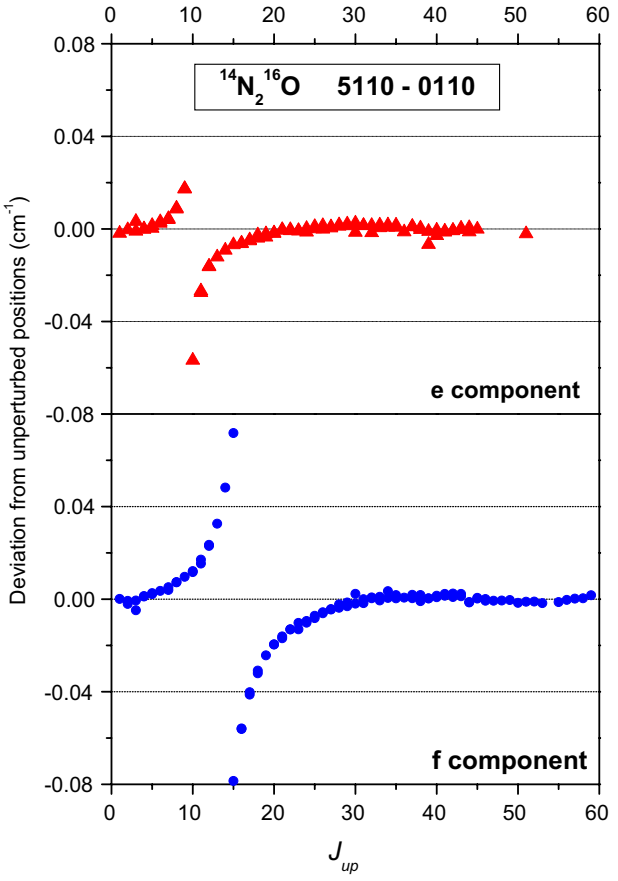

Fig. 6. Difference between the observed energy levels of the *e* and *f* components of the (11 1 11) state of $^{14}N_2{}^{16}O$, with the values calculated using the spectroscopic parameters of Table 2, versus the *J* rotational quantum number. The upper and lower panels are relative to the *e* and *f* sub bands, respectively. For each J_{upper} value, the values of the energy level obtained from the R($J_{upper}-1$) and P($J_{upper}+1$) transitions of the (11 1 11)–(1 1 1) (5110–0110 in the normal modes notations) Π–Π hot band at 6303.46 cm^{-1} are plotted but they are hardly distinguishable at the used energy scale. The Coriolis interaction of the (11 1 11) state with the (12 2 12) dark state is responsible for the perturbation of the rovibrational states near the energy crossing at $J = 15$ and $J = 10$, observed for the *f* and *e* component, respectively.

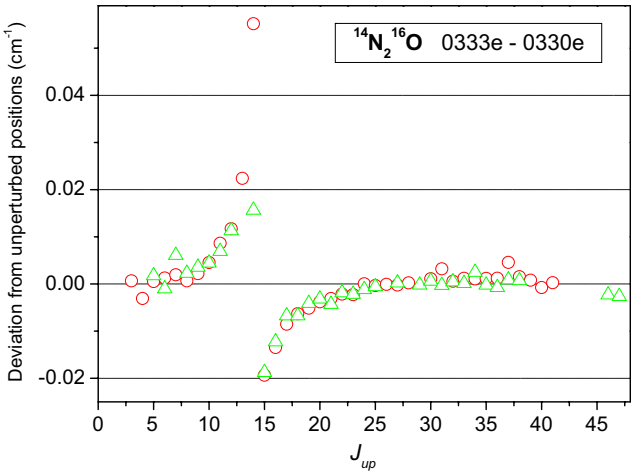

Fig. 7. Same as Fig. 6 for the (15 3 2) state of $^{14}N_2{}^{16}O$ observed through the (15 3 2)–(3 3 2) (0333e–0330e in normal modes notations) Φ–Φ hot band at 6453.89 cm^{-1}. For each J_{upper} value, the values of the energy level obtained from the R($J_{upper}-1$) and P($J_{upper}+1$) transitions are marked with open triangle and open square, respectively. The anharmonic interaction of the (15 3 2) state with the (13 3 27) dark state is responsible for the perturbation of the rovibrational states near the energy crossing at $J = 15$.

indicated in the last column, the corresponding bands and reference of these previous observations.

Two of the analyzed bands, corresponding to the (15 3 2) and (11 1 11) states, were found to present local perturbations in their rotational structure. Figs. 6 and 7 show the deviation from their respective unperturbed positions as calculated from the parameters of Table 2. The perturbation of the (15 3 2) state around $J' = 15$ results from an anharmonic interaction with the (13 3 27) state (J' is the angular momentum quantum number of the upper state of a transition). As discussed in Ref. [18] the energy levels of the (11 1 11) state are affected by a Coriolis interaction with the (12 2 12) state. For *J* values around the energy crossing, significant differences are noted between our line positions and those published in Ref. [18]. Our values satisfy the lower state combination differences relations and the perturbations strongly follow the predicted energy level crossings (see below) while only lines of the *P* branch were reported in Ref. [18] in the region of the local perturbation.

3.2.2. The 456, 546, 448 and 447 minor isotopologues

Wang et al. [18] detected the $3\nu_3$ band of 456 in the FTS spectrum of natural nitrous oxide. The examination of previous studies, in particular the reports of Toth [15] and Amiot [19,20], shows that further observations relative to these species were inexistent above 6000 cm^{-1}. However, the 456 and 546 FTS spectra have been very recently obtained in Hefei by using samples with a high isotopic enrichment. The results of the analysis of these spectra between 4000 and 9000 cm^{-1} will be presented in a separate contribution. A total of 17 bands of these four minor isotopologues are newly observed in our sample in natural abundance. The spectroscopic parameters relative to the 456, 546, 447 and 448 species are presented in Tables 3–6, respectively.

The 456 rotational levels of the (12 0 7) vibrational state are affected by a perturbation around $J' = 22$. This perturbation is due to an intrapolyad resonance interaction but our preliminary set of the effective Hamiltonian parameters does not allow identifying unambiguously the perturber. The spectroscopic parameters values for this band, listed in Table 3, were obtained by including low J' values ($J' < 22$). As illustrated by the deviations from the unperturbed positions (Fig. 8), a different set of rovibrational constants can be obtained by a fit reproducing the levels with J' values higher than 26. It leads to a difference of

Table 3
Spectroscopic parameters (in cm^{-1}) of the rovibrational bands of $^{14}N^{15}N^{16}O$ recorded by *CW*-CRDS between 6100 and 6833 cm^{-1}

Lower states constants [15]									
State				G_v	B_v				$D_v \times 10^7$
$V_1 V_2^{l_2} V_3$			(P, l_2, i)						
0000e			(0 0 1)	0.0	0.418 981 810				1.763264
0110*e*			(1 1 1)	575.43365	0.419 089 600				1.785826
0110f				575.43365	0.419 918 641				1.794459
ΔG_v [a]	Type	$V_1 V_2^{l_2} V_3$ [b]	(P, l_2, i)	G_v	B_v	$D_v \times 10^7$	Observed lines	n/N [c]	rms $\times 10^3$
Cold bands									
6121.7313(14)	Σ–Σ	4200e–0000e	(10 0 10)	6121.7313(14)	0.4149423(39)	4.007 (23)	R38	24/26	1.0
6240.66496(25)	Σ–Σ	5000e–0000e (3400e–0000e)	(10 0 11)	6240.66496(25)	0.41246940(79)	2.4543(44)	P42/R45	70/76	1.2
6322.99842(26)	Σ–Σ	5000e–0000e	(10 0 12)	6322.99842(26)	0.41039030(70)	1.1568(34)	P44/R48	68/71	1.1
6446.89417(18)	Σ–Σ	0003e–0000e	(12 0 1)	6446.89417(18)	0.40897230(31)	1.74229(94)	P58/R60	106/109	1.0
		0003e–0000e [Wa]		*6446.89423*	*0.4089692*	*1.730*			
6653.94605(60)	Σ–Σ	1202e–0000e	(12 0 5)	6653.94605(60)	0.4115745(23)	2.605(17)	P39/R38	48/50	1.9
6775.22182(33)	Σ–Σ	2002e–0000e (perturbed)	(12 0 7)	6775.22182(33)	0.4085965(38)	1.266(81)	P46/R47	35/79	1.0
Hot bands									
6406.42319(43)	Π–Π	0113e–0110e	(13 1 2)	6981.85684(43)	0.40922940(98)	1.7627(43)	P39/R49	62/70	1.7
6406.42113(39)		0113f–0110f		6981.85478(39)	0.40999680(88)	1.7728(37)	P39/R52	67/74	1.7

Notes. The parameters of the lower levels are taken from Ref. [15]. The uncertainties are given in parenthesis in the unit of the last quoted digit.
[Wa] Wang et al. [18].
[a] Difference between the upper and lower vibrational term values.
[b] Normal mode labeling according to the maximum value of the modulo of the expansion coefficients of an eigenfunction.
[c] n, number of transitions included in the fit; N, number of assigned rotational transitions.

Table 4
Spectroscopic parameters (in cm^{-1}) of the rovibrational bands of $^{15}N^{14}N^{16}O$ recorded by *CW*-CRDS between 6100 and 6833 cm^{-1}

Lower states constants [15]									
State				G_v	B_v				$D_v \times 10^7$
$V_1 V_2^{l_2} V_3$			(P, l_2, i)						
0000e			(0 0 1)	0.0	0.404857965				1.642938
0110*e*			(1 1 1)	585.31212	0.405037265				1.656798
0110f				585.31212	0.405781109				1.667421
ΔG_v [a]	Type	$V_1 V_2^{l_2} V_3$ [b]	(P, l_2, i)	G_v	B_v	$D_v \times 10^7$	Observed lines	n/N [c]	rms $\times 10^3$
Cold bands									
6135.36591(33)	Σ–Σ	0(10)00e–0000e	(10 0 10)	6135.36591(33)	0.4009625(17)	2.859 (15)	P4/R34	33/36	1.6
6232.91734(34)	Σ–Σ	5000e–0000e	(10 0 11)	6232.91734(34)	0.39871840(87)	1.6093(38)	P49/R49	83/89	1.7
6315.01651(38)	Σ–Σ	3400e–0000e	(10 0 12)	6315.01651(38)	0.3994122(11)	0.2073(54)	P46/R46	59/64	1.4
6515.98762(20)	Σ–Σ	0003e–0000e	(12 0 1)	6515.98762(20)	0.39475860(42)	1.6185(16)	P58/R45	77/85	1.0
6702.35285(31)	Σ–Σ	0402e–0000e	(12 0 5)	6702.35285(31)	0.39744770(88)	2.0975(47)	P37/R46	71/76	1.4
6795.93260(26)	Σ–Σ	2002e–0000e	(12 0 6)	6795.93260(26)	0.39501620(57)	1.4269(23)	P52/R50	79/80	1.2
Hot bands									
6473.43530(54)	Π–Π	0113e–0110e	(13 1 1)	7058.74742(54)	0.3950686(14)	1.6477(61)	P50/R43	67/71	2.2
6473.43182(59)		0113f–0110f		7058.74394(59)	0.3957746(15)	1.6557(68)	P50/R43	57/65	2.3

Notes. H_v parameters were constrained to the lower state values [15]. The uncertainties are given in parenthesis in the unit of the last quoted digit.
[a] Difference between the upper and lower vibrational term values.
[b] Normal mode labeling according to the maximum value of the modulo of the expansion coefficients of an eigenfunction.
[c] n, number of transitions included in the fit; N, number of assigned rotational transitions.

0.0333 cm^{-1} between the two effective values of the vibrational term.

In spite of the high number of lines which could be assigned, more than 3000 additional lines were left unassigned after the identification of the lines due to H_2O and CO_2, present as impurities in our sample. No doubt that a significant percentage of these lines, which are all relatively weak, are transitions of the different isotopologues

Table 5
Spectroscopic parameters (in cm^{-1}) of the rovibrational bands of $^{14}N_2{}^{18}O$ recorded by *CW*-CRDS between 6100 and 6833 cm^{-1}

Lower state constants [15]									
$V_1 V_2^{l_2} V_3$			(P, l_2, i)		G_v		B_v		$D_v \times 10^7$
0000e			(0 0 1)		0.0		0.395577895		1.583456
ΔG_v [a]	Type	$V_1 V_2^{l_2} V_3$ [b]	(P, l_2, i)	G_v	B_v	$D_v \times 10^7$	Observed lines	n/N [c]	rms $\times 10^3$
6140.55484(34)	Σ–Σ	5000e–0000e	(10 0 11)	6140.55484(34)	0.3899166(12)	0.9058(69)	P10/R43	45/45	1.4
6558.67369(21)	Σ–Σ	0003e–0000e	(12 0 1)	6558.67369(21)	0.3859087(5)	1.6244(23)	P49/R50	75/77	1.0
6702.93279(23)	Σ–Σ	1202e–0000e	(12 0 4)	6702.93279(23)	0.3881574(9)	2.0361(66)	P40/R39	63/65	1.0

Notes. The uncertainties are given in parenthesis in the unit of the last quoted digit.
[a] Difference between the upper and lower vibrational term values.
[b] Normal mode labeling according to the maximum value of the modulo of the expansion coefficients of an eigenfunction.
[c] n, number of transitions included in the fit; N, number of assigned rotational transitions.

Table 6
Spectroscopic parameters (in cm^{-1}) of the $3\nu_3$ band of $^{14}N_2{}^{17}O$ recorded by *CW*-CRDS

Lower state constants [15]									
$V_1 V_2^{l_2} V_3$			(P, l_2, i)		G_v		B_v		$D_v \times 10^7$
0000e			(0 0 1)		0.0		0.406672154		1.663972
ΔG_v [a]	Type	$V_1 V_2^{l_2} V_3$ [b]	(P, l_2, i)	G_v	B_v	$D_v \times 10^7$	Observed lines	n/N [c]	rms $\times 10^3$
6569.48825(31)	Σ–Σ	0003e–0000e	(12 0 1)	6569.48825(31)	0.3966566(10)	1.6526(58)	P44/R34	60/61	1.2

Notes. The uncertainties are given in parenthesis in the unit of the last quoted digit.
[a] Difference between the upper and lower vibrational term values.
[b] Normal mode labeling according to the maximum value of the modulo of the expansion coefficients of an eigenfunction.
[c] n, number of transitions included in the fit; N, number of assigned rotational transitions.

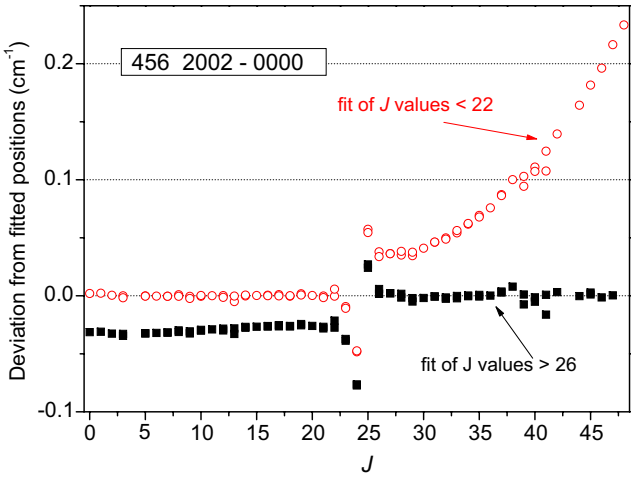

Fig. 8. Same as Fig. 6 for the (12 0 7) state of $^{14}N^{15}N^{16}O$ observed through the (12 0 7)–(0 0 0) (2002e–0000e in normal modes notations) Σ–Σ band at 6775.22 cm^{-1}. For each J_{upper} value, the values of the energy level obtained from the R($J_{upper}-1$) and P($J_{upper}+1$) transitions are plotted but they are hardly distinguishable at the used energy scale. The energy crossing observed around $J=24$ is due to an intrapolyad interaction with a still unidentified dark state. The residuals of two fits of the spectroscopic parameters are presented: the open circles correspond to the fit of the lower energy levels ($J<22$) leading to the parameters values listed in Table 3, while the full squares correspond to the fit of the higher energy levels ($J>26$).

of nitrous oxide which deviate significantly from their predicted positions.

4. Discussion

The (obs.-pred.) deviations of the line positions of the 446 isotopologue assigned in the studied region are displayed on Fig. 9. This figure demonstrates a good predictive ability of the effective Hamiltonian parameters [9–11] of the 446 isotopologue since the majority of the residuals lies between −0.04 and 0.04 cm^{-1}. However, our goal is a modelling of the line positions at the accuracy level of 0.001 cm^{-1}. In this respect, the new observed line positions will be very useful to improve the set of effective Hamiltonian parameters for this isotopic species.

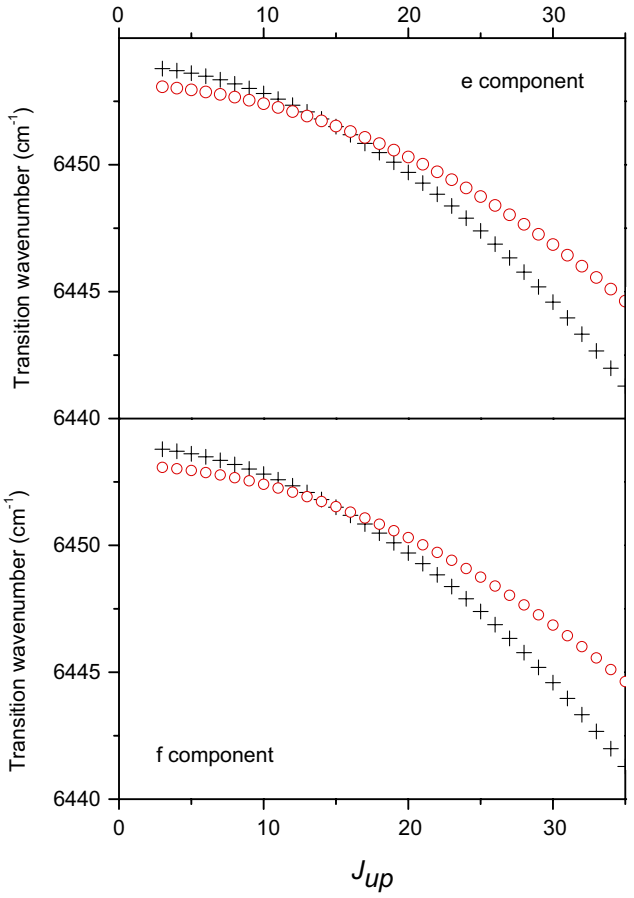

Fig. 10. Plot of the difference between the energy of the J levels of the (1532) and (13327) states with that of the (332) state of $^{14}N_2{}^{16}O$, as predicted by the polyad model of effective Hamiltonian [10]. The upper and lower panel corresponds to the e and f sub band, respectively. The energy crossing predicted around $J=15$ accounts of the local perturbation observed for the (1532)–(332) band (see Fig. 7 and text). The crosses (+) and open circles (○) correspond to the (1532) bright state and (13327) dark state, respectively.

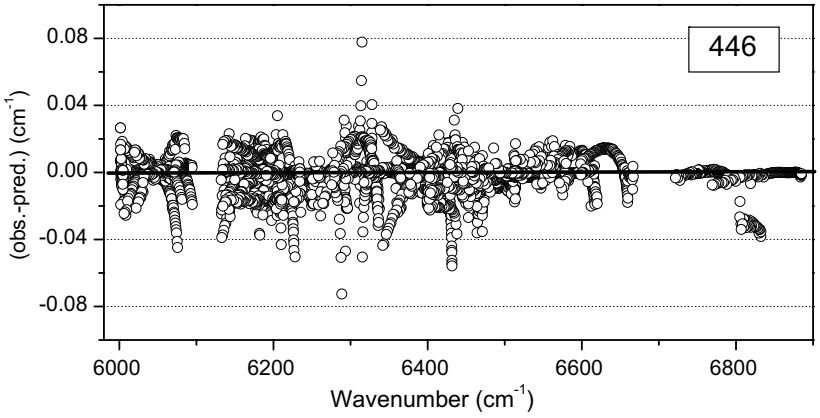

Fig. 9. Difference between the line positions of the 446 isotopologue of nitrous oxide assigned in the CW-CRDS spectrum between 6000 and 6833 cm^{-1} and their values predicted by the effective rovibrational Hamiltonian [10].

Due to a lack of input experimental information, many important parameters are absent in the preliminary sets of effective Hamiltonian that we could obtain for the 456 and 546 isotopologues. As a result, the deviations of the observed line positions from those predicted exceed 1 cm^{-1} for one of the 456 bands and in the case of 546 isotopologue, reach a value of 15 cm^{-1}. No doubt that the present results together with the recent FTS spectra obtained at Hefei with high isotopic enrichment will help to greatly improve the respective sets of effective Hamiltonian parameters.

Let us underline that all the predicted line positions have been obtained using the *polyad model* of effective Hamiltonian, while as already evidenced in our previous papers [18,22–24], two local perturbations due to *interpolyad* resonance interactions were identified for the 446 isotopologue. The (11 1 11)–(1 1 1) band, which was firstly observed in Ref. [18], is in resonance Coriolis interaction with the (12 2 12)–(1 1 1) band while the (15 3 2)–(3 3 2) band is in resonance anharmonic interaction with the (13 3 27)–(3 3 2) band. The plot of the crossing of the unperturbed energy levels for the (11 1 11) and (12 2 12) vibrational states is presented in Fig. 4 of Ref. [18]. We present in Fig. 10, the respective plot for the (1532) and (13327) vibrational states.

These two interpolyad Coriolis and anharmonic resonance interactions could be taken into account within the framework of the *nonpolyad* model of effective Hamiltonian by involving the matrix elements of the Coriolis interaction operators:

$$\langle V_1\ V_2^{\ell_2}\ V_3\ J\ K|H^{\mathrm{eff}}|V_1-1(V_2-1)^{\ell_2\pm1}\ V_3+1\ J\ K\pm1\rangle,$$
$$\langle V_1\ V_2^{\ell_2}\ V_3\ J\ K|H^{\mathrm{eff}}|V_1(V_2-3)^{\ell_2\pm1}\ V_3+1\ J\ K\pm1\rangle,$$
$$\langle V_1\ V_2^{\ell_2}\ V_3\ J\ K|H^{\mathrm{eff}}|V_1+2(V_2-1)^{\ell_2\pm1}\ V_3-1\ J\ K\pm1\rangle,$$

and anharmonic interaction operators:

$$\langle V_1\ V_2^{\ell_2}\ V_3\ J\ K|H^{\mathrm{eff}}|V_1+3V_2^{\ell_2}\ V_3-2\ J\ K\rangle,$$
$$\langle V_1\ V_2^{\ell_2}\ V_3\ J\ K|H^{\mathrm{eff}}|V_1+2(V_2+2)^{\ell_2}\ V_3-2\ J\ K\rangle.$$

5. Conclusion

New experimental information about the rovibrational transitions of N_2O near 1.5 μm has been obtained with a CW-CRDS spectrometer using a series of 40 DFB lasers allowing for a continuous coverage of the 6000–6900 cm^{-1} spectral region. The band by band analysis has led to the determination of the rovibrational parameters of a total of 68 bands due to five isotopologues, 446, 456, 546, 448 and 447. The rovibrationally assignment was performed on the basis of the predictions of the global effective Hamiltonian models which show an overall good agreement with the observations for the 446 isotopologue. However, the relatively high percentage of lines left unassigned, points a possible bias of the assignment procedure: as a result of the very high density of lines detected by CRDS (typically 10–20 lines/cm^{-1}), we have probably failed in assigning some of the observed lines when the EH predictions show unusually large deviations from the observations. The present new data will be used to refine the set of parameters of the effective Hamiltonian models and to improve the quality of the predictions. It will probably help to significantly reduce the amount of unassigned transitions. In particular, a significant improvement is expected from the development of a new nonpolyad model of effective Hamiltonian which will take into account interpolyad resonance interactions as these interactions play an important role in the nitrous oxide molecule [15,18,22–24].

Acknowledgments

This work, performed in the frame of the European research network QUASAAR (MRTN-CT-2004-512202), is jointly supported by a collaborative project between CNRS-France and RFBR-Russia (PICS Grant No 05-05-22001) and between CNRS and CAS-China (PICS Grant No 3359). The support of the Programme National LEFE (CHAT) INSU-CNRS is acknowledged.

Appendix A. Supplementary data

Supplementary data for this article are available on ScienceDirect (www.sciencedirect.com) and as part of the Ohio State Univeristy Molecular Spectroscopy Archives (http://msa.lib.ohio-state.edu/jmsa_hp.htm).

References

[1] P. Macko, D. Romanini, S.N. Mikhalenko, O.V. Naumenko, S. Kassi, A. Jenouvrier, Vl.G. Tyuterev, A. Campargue, J. Mol. Spectrosc. 227 (2004) 90–108.
[2] Z. Majcherova, P. Macko, D. Romanini, V. Perevalov, S.A. Tashkun, J.-L. Teffo, A. Campargue, J. Mol. Spectrosc. 230 (2005) 1–21.
[3] B.V. Perevalov, S. Kassi, D. Romanini, V.I. Perevalov, S.A. Tashkun, A. Campargue, J. Mol. Spectrosc. 238 (2006) 241–255.
[4] Y. Ding, P. Macko, D. Romanini, V. Perevalov, S.A. Tashkun, J.-L. Teffo, S.-M. Hu, A. Campargue, J. Mol. Spectrosc. 226 (2004) 146–160.
[5] M.-R. De Backer-Barilly, Vl.G. Tyuterev, D. Romanini, B. Moeskops, A. Campargue, J. Mol. Struct. 780–781 (2005) 225–233.
[6] A. Campargue, S. Kassi, D. Romanini, A. Barbe, M.-R. De Backer-Barilly, Vl.G. Tyuterev, J. Mol. Spectrosc. 240 (2006) 1–13.
[7] M.A.K. Khalil, R.A. Rasmussen, J. Geophys. Res. 97 (1992) 14651, 1460.
[8] L.S. Rothman, D. Jacquemart, A. Barbe, D.C. Benner, M. Birk, L.R. Brown, M.R. Carleer, C. Chackerian Jr., K. Chance, L.H. Coudert, V. Dana, V.M. Devi, J.-M. Flaud, R.R. Gamache, A. Goldman, J.-M. Hartmann, K.W. Jucks, A.G. Maki, J.-Y. Mandin, S.T. Massie, J. Orphal, A. Perrin, C.P. Rinsland, M.A.H. Smith, J. Tennyson, R.N. Tolchenov, R.A. Toth, J. Vander Auwera, P. Varanasi, G. Wagner, J. Quant, Spectrosc. Radiat. Transfer 96 (2005) 139–204.
[9] J.-L. Teffo, V.I. Perevalov, O.M. Lyulin, J. Mol. Spectrosc. 168 (1994) 390–403.
[10] V.I. Perevalov, S.A. Tashkun, J.-L. Teffo, Sixteenth Colloquium on High Resolution Molecular Spectroscopy, Dijon (France). 6–10 September 1999, Poster D2, p. 103.
[11] A.V. Vlasova, B.V. Perevalov, S.A. Tashkun, V.I. Perevalov, Proc. SPIE 6580 (2006) 658007.

[12] J. Morville, D. Romanini, A.A. Kachanov, M. Chenevier, Appl. Phys. B 78 (2004) 465–476.
[13] R.A. Toth, available from: <http://mark4sun.jpl.nasa.gov/n2o.html>.
[14] C. Amiot, G. Guelachvili, J. Mol. Spectrosc. 51 (1974) 475–491.
[15] R.A. Toth, J. Mol. Spectrosc. 197 (1999) 158–187.
[16] G. Weirauch, A.A. Kachanov, A. Campargue, M. Bach, J. Vander Auwera, M. Herman, J. Mol. Spectrosc. 202 (2000) 98–106.
[17] H. Oshika, A. Toba, M. Fujitake, N. Ohashi, J. Mol. Spectrosc. 197 (1999) 324.
[18] L. Wang, V.I. Perevalov, S.A. Tashkun, B. Gao, L.-Y. Hao, S.–M. Hu, J. Mol. Spectrosc. 237 (2006) 129–136.
[19] C. Amiot, J. Mol. Spectrosc. 59 (1976) 191–208.
[20] C. Amiot, J. Mol. Spectrosc. 59 (1976) 380–395.
[21] L. Daumont, J. Vander Auwera, J.-L. Teffo, V.I. Perevalov, S.A. Tashkun, J. Quant. Spectrosc. Radiat. Transfer 104 (2007) 342–356.
[22] A. Campargue, G. Weirauch, S. Tashkun, V. Perevalov, J.-L. Teffo, J. Mol. Spectrosc. 209 (2001) 198–206.
[23] Y. Ding, V.I. Perevalov, S.A. Tashkun, J.-L. Teffo, S. Hu, E. Bertseva, A. Campargue, J. Mol. Spectrosc. 220 (2003) 80–86.
[24] E. Bertseva, A. Campargue, V.I. Perevalov, S.A. Tashkun, J. Mol. Spectrosc. 226 (2004) 196–200.